BIOLOGY OF REPRODUCTION **84,** 1225–1234 (2011)
Published online before print 3 February 2011.
DOI 10.1095/biolreprod.110.088955

The Testis-Enriched Histone Demethylase, KDM4D, Regulates Methylation of Histone H3 Lysine 9 During Spermatogenesis in the Mouse but Is Dispensable for Fertility[1]

Naoki Iwamori,[2,4] Ming Zhao,[7] Marvin L. Meistrich,[7] and Martin M. Matzuk[3,4,5,6]

Departments of Pathology and Immunology,[4] Molecular and Cellular Biology,[5] and Molecular Human Genetics,[6] Baylor College of Medicine, Houston, Texas
Department of Experimental Radiation Oncology,[7] University of Texas M.D. Anderson Cancer Center, Houston, Texas

ABSTRACT

Epigenetic modifications, and methylation of histones in particular, dynamically change during spermatogenesis. Among various methylations of histone H3, methylation of histone H3 lysine 9 (H3K9) and its regulation are essential for spermatogenesis. Trimethytransferases as well as dimethyltransferase are required for meiotic progression. In addition, didemethylase of H3K9 is also critical for spermatogenesis through transcriptional regulation of spermatid-specific genes. However, the requirement for demethylation of trimethylated H3K9 (H3K9me3) during spermatogenesis remains to be elucidated. Here, we report the targeted disruption of KDM4D, a testis-enriched tridemethylase of H3K9. *Kdm4d*-null mice are viable and fertile and do not show any obvious phenotype. However, H3K9me3 accumulates significantly in *Kdm4d*-null round spermatids, and the distribution of methylated H3K9 in germ cells is dramatically changed. Nevertheless, the progression of spermatogenesis and the number of spermatozoa are normal, likely secondary to the earlier nuclear localization of another H3K9 tridemethylase, KDM4B, in *Kdm4d*-null elongating spermatids. These results suggest that demethylation of H3K9me3 in round spermatids is dispensable for spermatogenesis but that possible defects in *Kdm4d*-null elongating spermatids could be rescued by functional redundancy of the KDM4B demethylase.

epigenetics, gamete biology, histone demethylase, spermatogenesis, testis

INTRODUCTION

Genomic DNA is compacted in the nucleus as chromatin. The basal subunit of chromatin is a nucleosome, which consists of 146 bp of DNA wrapped around the octamer of core histones H2A, H2B, H3, and H4. The N-terminal tail of these four histones can be modified in several ways by phosphorylation, acetylation, methylation, and ubiquitination. Each modification is related to important cellular processes, including transcriptional regulation, heterochromatin formation, DNA recombination, DNA damage response, and X-chromosome inactivation [1–3].

Several lysines (K) of histone H3 and H4 (i.e., K4, K9, K27, K36, and K79 of histone H3 and K20 of histone H4) can be methylated in four distinct states—un-, mono- (me1), di- (me2), and trimethylated (me3)—and the methylation status of each lysine has independent functions [1, 4]. For example, methylated H3K4 and H3K36 are required for transcriptional activation, whereas methylated H3K9, H3K27, and H4K20 are necessary for transcriptional repression [3, 5]. Among the methylation patterns of histones, the dynamic changes of methylated H3K4 and H3K9 in the testicular germ cells during spermatogenesis have been reported [6–8].

A series of enzymes that catalyze the methylation of each lysine residue, histone lysine methyltransferases (KMTs) and histone lysine demethylases (KDMs), have been identified, and each enzyme has substrate specificity [3, 5]. Some of the enzymes that can catalyze methylation of H3K9 have been reported as being essential for spermatogenesis. Male germ cells that lack H3K9 trimethyltransferases (i.e., KMT1A/SUV39H1 and KMT1B/SUV39H2) show abnormal synapsis and missegregation of chromosomes in pachytene spermatocytes [9, 10]. Similarly, male germ cells lacking the H3K9 dimethyltransferase, KMT1C/G9a, demonstrate defects in meiotic prophase progression [11]. Alternatively, the H3K9 didemethylase, KDM3A/JHDM2A/JMJD1A, is critical for spermatogenesis through transcriptional regulation of *Tnp1* and *Prm1* expression, although the global distribution of H3K9me1/me2 in the seminiferous tubule was not affected [12]. To our knowledge, however, the role of demethylation of H3K9me3 remains to be elucidated.

In the present report, we show preferential expression of KDM4D (also known as JMJD2D), one of the tridemethylases of H3K9 in the testis. Two different reports have shown demethylase activity of KDM4D. One report showed that KDM4D could demethylate H3K9me1/me2/me3, whereas the other indicated that KDM4D could demethylate H3K9me2/me3 but not H3K9me1 [13, 14]. Using a mouse knockout model, loss of demethylation by KDM4D does not affect the completion of spermatogenesis or fertility, despite dramatic changes in the distribution of mono-, di-, and trimethylated H3K9 in $Kdm4d^{-/-}$ testis. We hypothesize that the lack of fertility defects in $Kdm4d^{-/-}$ mice is rescued by functional redundancy with another KDM4 protein, KDM4B (also known as JMJD2B).

MATERIALS AND METHODS

Semiquantitative RT-PCR

Total RNA from adult mouse tissue samples was extracted using TRIzol (Invitrogen) according to the manufacturer's instruction and reverse transcribed using Superscript III reverse transcriptase and an oligo-dT primer (Invitrogen). The primers to amplify the *Kdm4d* cDNA fragment spanning exons 1 and 2

[1]Supported in part by National Institutes of Health grant R01HD057880.
[2]Correspondence: Naoki Iwamori, Department of Pathology and Immunology, Baylor College of Medicine, One Baylor Plaza, Houston, TX 77030. FAX: 713 798 5833; e-mail: iwamori@bcm.tmc.edu
[3]Correspondence: Martin M. Matzuk, Department of Pathology and Immunology, Baylor College of Medicine, One Baylor Plaza, Houston, TX 77030. FAX: 713 798 5833; e-mail: mmatzuk@bcm.tmc.edu

Received: 5 October 2010
First decision: 14 November 2010
Accepted: 28 January 2011
© 2011 by the Society for the Study of Reproduction, Inc.
eISSN: 1529-7268 http://www.biolreprod.org
ISSN: 0006-3363

Downloaded from www.biolreprod.org.

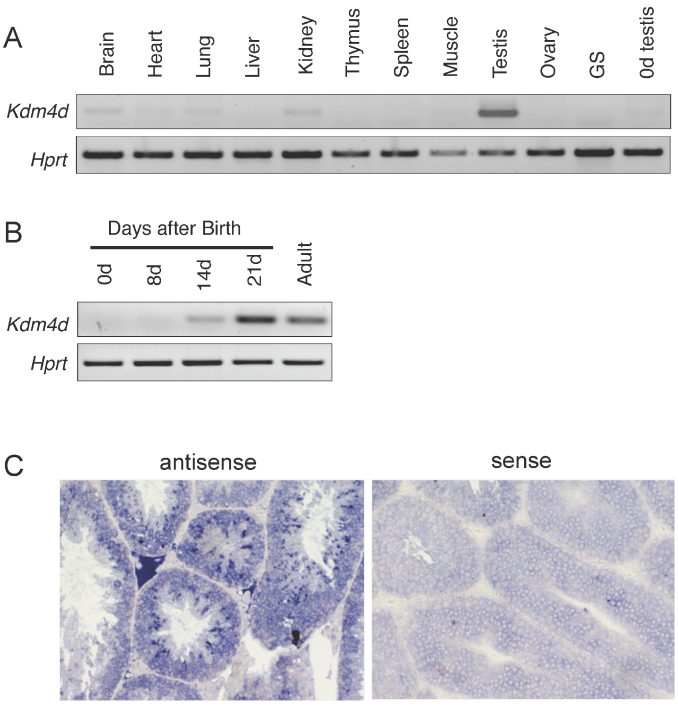

FIG. 1. Spatiotemporal expression of *Kdm4d*. **A** and **B**) Transcripts of *Kdm4d* were examined by semiquantitative RT-PCR in multiple tissue samples (**A**) and during postnatal development of the testis (**B**). *Hprt* was used as an internal control. GS, germline stem cells. **C**) In situ hybridization of *Kdm4d*. An antisense probe (**left**) and a sense probe (**right**) specific for *Kdm4d* were hybridized.

were as follows: forward, 5′-GGCTCCTGCTCCTCAGTAGA-3′; reverse, 5′-CTAACCCAGAGCCCAGCACTC-3′. *Hprt* served as an internal control and was amplified with following primers: forward, 5′-GTTCTTT GCTGACCTGCTGGA-3′; reverse, 5′-GGCCACAGGACTAGAACACC-3′.

Histology and In Situ Hybridization

Testes were fixed in Bouin fixative or 4% paraformaldehyde overnight, followed by paraffin embedding. Tissue embedding was performed by the Department of Pathology Histology Core, Baylor College of Medicine. Sections (thickness, 5 μm) were stained with periodic acid-Schiff reagent and counterstained with hematoxylin. In situ hybridization was performed on a section of paraformaldehyde-fixed tissues with a 411-bp, digoxigenin-labeled cRNA probe specific for *Kdm4d*. Sections (thickness, 5 μm) were treated with 2 μg/ml of proteinase K for 10 min and acetylated with acetylation buffer (100 mM triethanolamine and 0.25% acetic acid) for 20 min. After prehybridization with hybridization buffer (50% formamide, 4× SSC [1× SSC: 0.15 M sodium chloride and 0.015 M sodium citrate], 500 μg/ml of heparin, and 200 μg/ml of tRNA) for 60 min at 65°C, sections were hybridized with 300 ng/ml of probe containing hybridization buffer overnight at 65°C. The hybridized probe was detected by alkaline phosphatase-conjugated anti-digoxigenin antibody (Roche) using an alkaline phosphatase substrate kit (Vector Laboratories) according to the manufacturer's instructions.

Cell Culture, Plasmid Constructions, and Transfection

HeLa cells were maintained in Dulbecco modified Eagle medium supplemented with 10% fetal calf serum at 37°C in 5% CO_2 in air. The open reading frame (ORF) of KDM4D was subcloned into pcDNA3.1 with mCherry fluorescent protein in frame to make an mCherry-KDM4D fusion protein. Expression vectors pcDNA3.1-mCherry/*Kdm4d* and pcDNA3.1-mCherry were transfected into HeLa cells using fugene 6 reagent (Roche) according to the manufacturer's instructions. At 72 h after transfection, cells were subjected to histone extraction, followed by immunoblot analysis. For immunofluorescence, cells were replated at low density 24 h after transfection and analyzed 48 h after replating.

Histone Extraction and Immunoblot

The nuclear fraction was collected after cell lysis in the following buffer: 100 mM Tris/HCl [pH 7.5], 1.5 M NaCl, 1.5 mM $MgCl_2$, 0.65% NP-40, and protease inhibitor cocktail. Histones were extracted from the nuclear fraction by treatment with 0.2 M H_2SO_4, followed by trichloro-acetic acid agglutination and immunoblot analysis. Individual membranes were used to detect the methylation status of histone H3. Antibodies used for immunoblotting were as follows: anti-H3K4me3, anti-H3K9me1, anti-H3K9me2, anti-H3K9me3, and anti-H3K36me3 (all from Abcam) as well as anti-pan-histone H3 and anti-acetylated histone H3 (both from Millipore).

Immunofluorescence

Cells were fixed with 2% parafomaldehyde for 10 min and permeabilized with 0.5% NP-40 for 15 min. After incubation with primary antibodies for 2 h at room temperature, the methylation status of histone H3 was visualized by Alexa 488-conjugated anti-mouse immunoglobulin (Ig) G or anti-rabbit IgG antibodies (Invitrogen). For immunofluorescence of tissue sections, paraformaldehyde-fixed sections were retrieved by microwave (1250 W for 15 min in 0.1 M sodium citrate buffer [pH 6.0]), then incubated with primary antibody overnight at 4°C, followed by Alexa 488- and Alexa 594-conjugated secondary antibodies (Invitrogen) for 1 h at room temperature. Fluorescent sections were mounted with VECTASHIELD containing 4′,6′-diamidino-2-phenylindole (DAPI; Vector Laboratories). Fluorescence intensity of methylated H3K9 in representative cells was quantified using Image J software (National Institutes of Health). Primary antibodies other than those described above were as follows: anti-H3K4me1, anti-H3K4me2, anti-H3K9me2, anti-H3K27me2, and anti-H3K27me3 (all from Millipore) as well as anti-H2AFX (Abcam).

Generation of Kdm4d Knockout Mice

A targeting construct was generated using a recombineering strategy [15, 16]. Briefly, 9.8 kb of the genomic region containing exon 2 of *Kdm4d* was retrieved from BAC bMQ 176I19 (Welcome Trust Sanger Institute) [17] and inserted into pBluescript SK containing diphtheria toxin A for negative selection (pDTA.3 kindly provided by Dr. Pumin Zhang, Baylor College of Medicine, Houston, TX). The ORF of *Kdm4d* was replaced by a *PGK1-Neo* cassette. The linearized targeting construct was electroporated into AB2.1 embryonic stem cells, which are derived from 129S7/SvEv strain mice. Embryonic stem cell clones were selected in M15 supplemented with 0.18 mg/ml of G418. Targeted clones were screened by Southern blot analysis using 5′ and 3′ probes. Two of the correctly targeted clones were expanded and injected into C57BL/6J blastocysts. Chimeric males were bred to C57BL/6J females to obtain heterozygous *Kdm4d* mutant mice ($Kdm4d^{+/-}$). Homozygous mutant mice ($Kdm4d^{-/-}$) were produced by intercrossing male and female $Kdm4d^{+/-}$ mice. Mice were genotyped by Southern blot analysis using the probe indicated in Figure 3A or PCR analysis using the following primers: wild-type/knockout forward, CTGGCTCTGGGTTAGTCAGC; wild-type reverse, CCAGGT GACCCACATTCCAC; knockout reverse, CCACTCCCACTGTCCTTTCC.

Fertility Analysis and Sperm Counts

Six-week-old $Kdm4d^{-/-}$ and $Kdm4d^{+/-}$ male littermates were individually bred to wild-type or $Kdm4d^{+/-}$ females. The number of litters and pups born per litter were monitored over a 9-mo period. All mouse experiments were performed on a C57BL/6J:129S7/SvEvBrd hybrid background in accordance with protocols approved by the Institutional Care and Use Committee of Baylor College of Medicine. Total epididymal sperm counts were performed as previously described [18].

Chromosomal Analysis

Chromosome spread analysis was performed as previously described [19]. The following primary antibodies were used for this experiment: anti-SCP3 (Santa Cruz Biotechnology), anti-H3K9me2 (Millipore), and anti-H3K9me3 (Abcam). Alexa 594-conjugated anti-mouse IgG and Alexa 488-conjugated anti-rabbit IgG (both from Invitrogen) and VECTASHIELD containing DAPI were also used.

Statistical Analysis

Data are presented as the mean ± SEM. Statistical significance was determined by Student *t*-test, and $P < 0.05$ was considered to be statistically significant.

Downloaded from www.biolreprod.org.

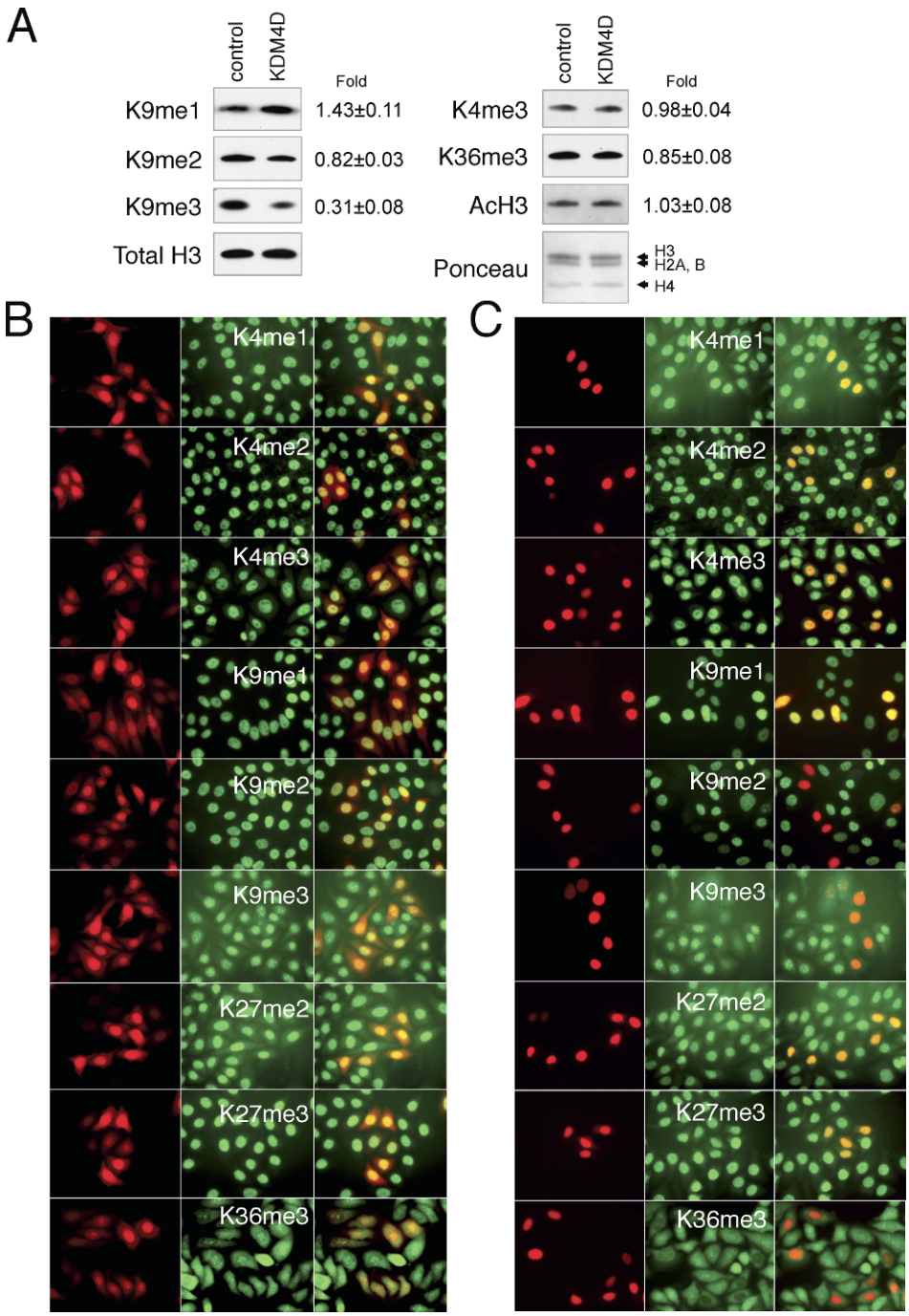

FIG. 2. Demethylation activity of KDM4D. **A**) Western blot of methylated histones in HeLa cells expressing KDM4D. Extracted histones from 1×10^5 HeLa cells expressing mCherry or mCherry-KDM4D were loaded. Fold-exchanges of each histone modification in KDM4D-expressing cells are indicated at the right of each picture. Ponceau staining is shown as a loading control. AcH3, acetylated histone H3. **B** and **C**) Immunostaining of methylated histones in HeLa cells expressing KDM4D. HeLa cells expressing mCherry (**B**) or mCherry-KDM4D (**C**) were fixed and stained with indicated antibodies. An mCherry or an mCherry-KDM4D (red; **left**), methylated histone (green; **middle**), and a merged image (**right**) are shown.

RESULTS

To identify the H3K9me3 demethylase that could be essential for spermatogenesis, expression of *Kdm4* genes were examined by analysis of the Expressed Sequence Tags (EST) database at the National Center for Biotechnology Information (NCBI) and the GNF (Genomics Institute of Novartis Research Foundation) BioGPS database [20], and in the process, *Kdm4d* was found as a testis-specific gene. To confirm the expression of *Kdm4d*, RT-PCR using RNA from multiple adult mouse tissues was performed. *Kdm4d* transcripts were detected at high levels in testis, as expected, but also at low levels in brain, heart, and kidney (Fig. 1A). The expression of *Kdm4d* in testis started at Postnatal Day 14 and increased with age (Fig. 1B). To define the precise expression of *Kdm4d*, in situ hybridization was performed and demonstrated that *Kdm4d* was expressed in spermatocytes and spermatids but not in spermatogonia and Sertoli cells (Fig. 1C). Lack of expression of *Kdm4d* in spermatogonia is consistent with lack of expression of *Kdm4d* in germline stem cells (Fig. 1A).

To evaluate the function of KDM4D and whether it can demethylate mono-, di-, and trimethylated H3K9, KDM4D was expressed in HeLa cells, and the methylation status of histone H3 was examined. H3K9me2 and H3K9me3 were decreased with KDM4D expression, whereas H3K9me1 was increased in KDM4D-expressing cells (Fig. 2A). Similar results were obtained by immunostaining experiments, which showed overexpression of an mCherry-KDM4D fusion protein (Fig. 2, B and C). Di- and trimethylated H3K9 disappeared from KDM4D-positive cells, whereas H3K9me1 were increased by

Downloaded from www.biolreprod.org.

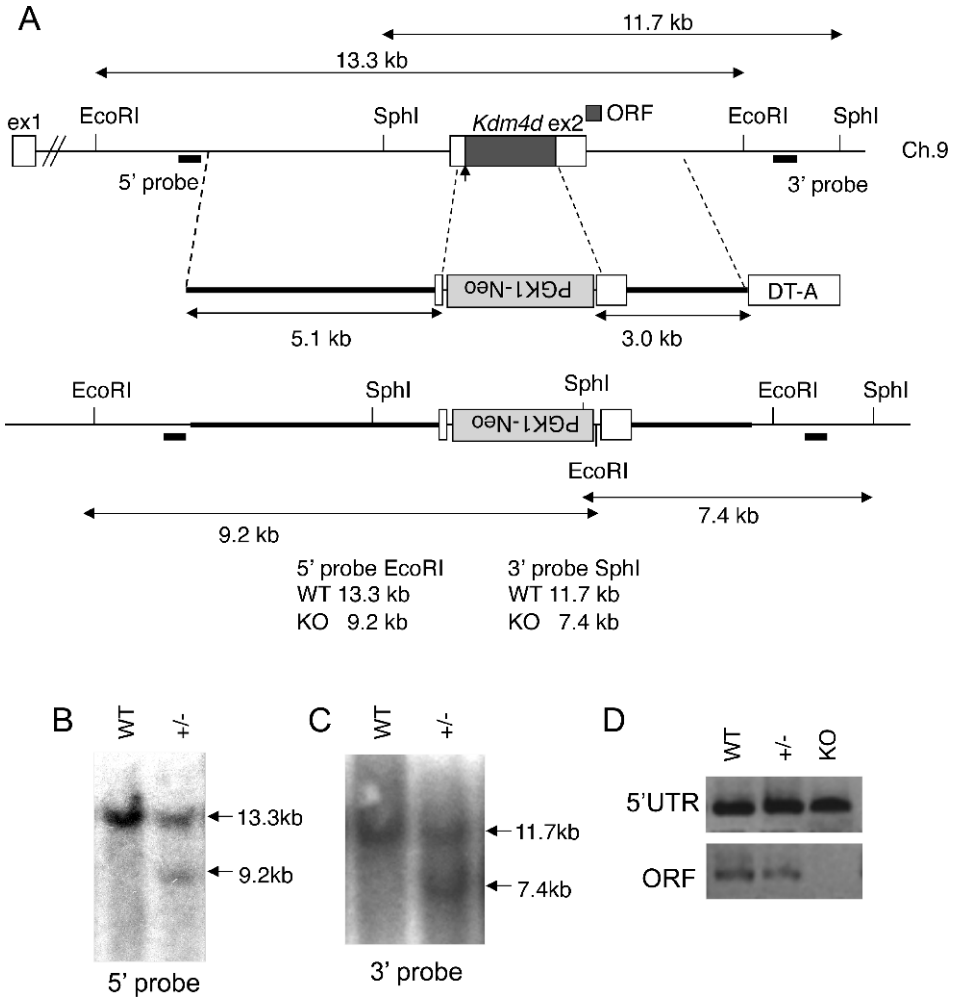

FIG. 3. Generation of *Kdm4d*-null mice. **A**) Strategy of targeting of the *Kdm4d* gene. The ORF of *Kdm4d* was replaced with a *PGK1-Neo* cassette. **B** and **C**) Southern blot analyses using 5′ (**B**) and 3′ (**C**) external probes. *Eco*RI-digested (**B**) and *Sph*I-digested (**C**) tail DNA were hybridized with probes that detect a 13.3-kb wild-type (WT) and 9.2-kb null alleles at the 5′ end (**B**) or an 11.7-kb WT and a 7.4-kb null alleles at the 3′ end (**C**). **D**) Confirmation of the *Kdm4d*-null allele. RT-PCR using primers spanning exon 1 and the 5′ untranslated region of exon 2 and primers within the ORF of *Kdm4d* are shown. DTA, diphtheria toxin fragment A; KO, knockout (homozygote); +/–, heterozygote.

KDM4D expression (Fig. 2C). Other methylation statuses of histone H3 did not change between KDM4D-negative and -positive cells except for H3K36me3 (Fig. 2). In cells with the highest expression of KDM4D, H3K9me1 was also demethylated (data not shown), but this finding was rare in our experiments. These results suggest that KDM4D can demethylate H3K9me2 and H3K9me3 into H3K9me1 without significant effects on most of the other histone H3 methylation patterns.

To address the in vivo functions of KDM4D, *Kdm4d* knockout mice were generated. We designed a targeting vector to delete the entire ORF of *Kdm4d* (Fig. 3A), because the entire ORF of *Kdm4d* is encoded by exon 2. A targeted allele of *Kdm4d* was generated in embryonic stem cells by homologous recombination. Successful recombination was verified by Southern blot analysis using both 5′ and 3′ external probes (Fig. 3, B and C). Male and female offspring from heterozygous intercrosses (n = 10) were born in an approximately 1:1 ratio (518 males [51.5%] and 487 females [48.5%]) with appropriate mendelian distribution (280 $Kdm4d^{+/+}$ [27.9%], 502 $Kdm4d^{+/-}$ [50.0%], and 223 $Kdm4d^{-/-}$ [22.2%]), indicating that deletion of *Kdm4d* does not affect viability. To confirm that our targeting strategy generated a null allele, RT-PCR using primer pairs between exons 1 and 2 and within the ORF of *Kdm4d* were performed (Fig. 3D). The 5′ untranslated region of *Kdm4d* was transcribed in $Kdm4d^{-/-}$ testis, but consistent with deletion, the ORF of *Kdm4d* was not detected in $Kdm4d^{-/-}$ testis, indicating that the *Kdm4d* mutant allele is a null allele.

To examine whether loss of KDM4D affected global H3K9 methylation during spermatogenesis, male germ cells were separated into pachytene spermatocytes, round spermatids, and elongated spermatids by an elutriation method [21, 22]. H3K9me3 was dramatically increased in $Kdm4d^{-/-}$ round spermatid, whereas H3K9me1 was decreased and H3K9me2 did not change in round spermatids (Fig. 4, A and B). Although H3K9me3 was not detected in $Kdm4d^{+/-}$ and $Kdm4d^{-/-}$ elongated spermatids, H3K9me2 and H3K9me1 were slightly elevated in $Kdm4d^{-/-}$ elongated spermatids (Fig. 4A). Methylation of other lysines of histone H3 was not changed in the absence of KDM4D (Fig. 4, A and B, and data not shown).

To further examine the distribution of methylated H3K9 in $Kdm4d^{-/-}$ testes, immunofluorescence staining was performed. The results showed dramatic alterations of global methylation of H3K9 in $Kdm4d^{-/-}$ testis. H3K9me3, which is a major target of KDM4D, forms foci at the center of each nucleus of round spermatids, whereas the H3K9me3 foci in $Kdm4d^{-/-}$ round spermatids were more intense at 2.07-fold (Fig. 4C and Supplemental Fig. S1; all Supplemental Data are available online at www.biolreprod.org). Immunoreactivities of H3K9me1 in round spermatids were decreased in $Kdm4d^{-/-}$ testis at 0.67-fold (Fig. 4C and Supplemental Fig. S1). On the other hand, H3K9me2 foci in round spermatids disappeared in $Kdm4d^{-/-}$ testes at both 3 and 10 wk of age (Fig. 4C and Supplemental Fig. S1). Distribution of H3K36me3 in $Kdm4d^{-/-}$ testis was also examined, because H3K36me3 was slightly affected by KDM4D expression (Fig. 2). No

Downloaded from www.biolreprod.org.

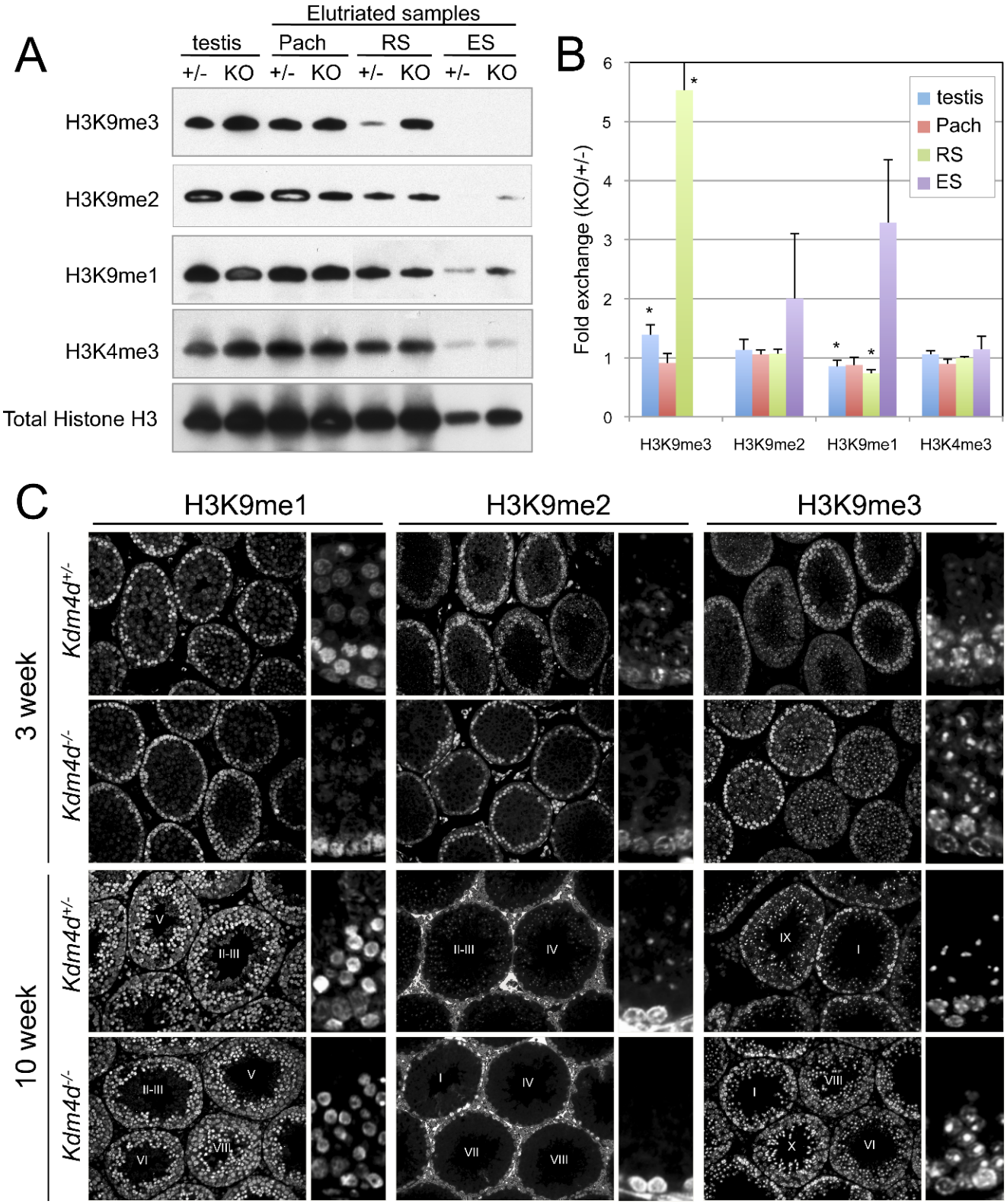

FIG. 4. Alterations in methylated histone H3 in *Kdm4d*$^{-/-}$ testis. **A**) Western blot analyses of H3K9me1, H3K9me2, H3K9me3, H3K4me3, and total histone H3 in *Kdm4d*$^{+/-}$ and *Kdm4d*$^{-/-}$ germ cell-enriched testes, pachytene spermatocytes (Pach), round spermatids (RS), and elongated spermatids (ES) are shown. **B**) Quantitative changes of H3K9me1, H3K9me2, H3K9me3, and H3K4me3 are shown in **A**. Relative fold-exchanges of H3K9me1, H3K9me2, H3K9me3, and H3K4me3 in *Kdm4d*$^{-/-}$ germ cells are shown. *$P < 0.05$. **C**) Low- and high-magnification of immunofluorescence images of H3K9me1, H3K9me2, and H3K9me3 in *Kdm4d*$^{+/-}$ and *Kdm4d*$^{-/-}$ testes at 3 wk and 10 wk of age. Roman numerals indicate spermatogenic stages.

Downloaded from www.biolreprod.org.

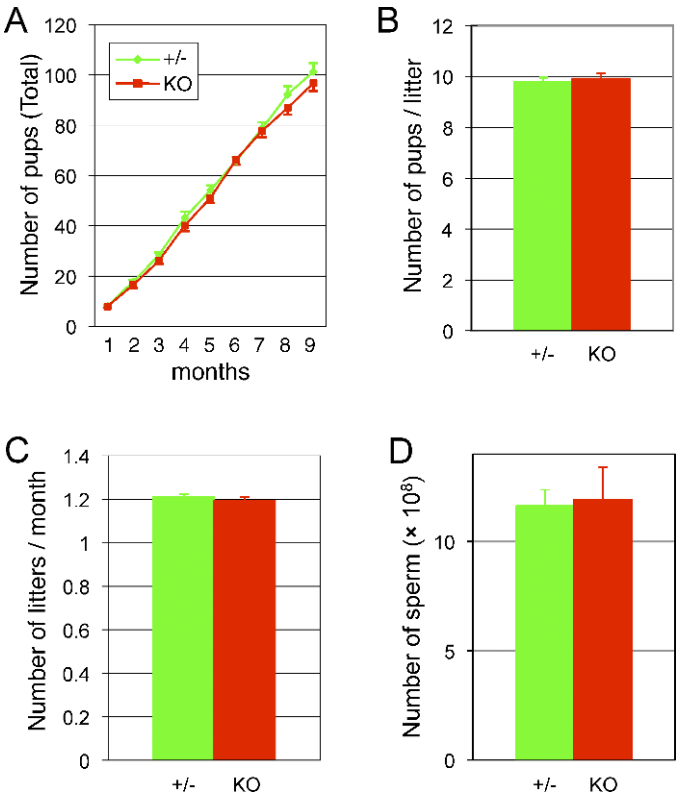

FIG. 5. Fertility analysis and sperm counts of *Kdm4d* knockout mice. **A**) Average number of pups produced by *Kdm4d*$^{+/-}$ (+/–) and *Kdm4d*$^{-/-}$ (KO) males over 9 mo of breeding (n = 10 per genotype). **B** and **C**) Average litter size (**B**) and litters per month (**C**) produced by *Kdm4d*$^{+/-}$ (+/–) and *Kdm4d*$^{-/-}$ (KO) males. **D**) Number of total epididymal sperm in 6-mo-old *Kdm4d*$^{+/-}$ and *Kdm4d*$^{-/-}$ males (n = 4 per genotype).

differences between *Kdm4d*$^{+/-}$ and *Kdm4d*$^{-/-}$ testes were detectable (Supplemental Fig. S2).

To assess the roles of KDM4D in male fertility, *Kdm4d*$^{+/-}$ and *Kdm4d*$^{-/-}$ males were mated with wild-type or *Kdm4d*$^{+/-}$ females on a mixed genetic background (B6; 129S7) beginning at 6 wk of age. Over the course of 9 mo of breeding, no significant differences were found in number of pups, litters per month, and pups per litter between *Kdm4d*$^{+/-}$ and *Kdm4d*$^{-/-}$ males (Fig. 5, A–C, and Table 1). In addition, the sperm count of each genotype was normal, suggesting that lack of KDM4D did not affect male fertility and completion of spermatogenesis (Fig. 5D). Although *Kdm4d*$^{-/-}$ testes were as big as *Kdm4d*$^{+/-}$ testis at 6 wk of age, the *Kdm4d*$^{-/-}$ testes were bigger than the *Kdm4d*$^{+/-}$ testes at 12 wk (Fig. 6, A and B). These differences in testis size were only transient, because the sizes of *Kdm4d*$^{+/-}$ and *Kdm4d*$^{-/-}$ testes were not statistically different at 1 yr (Fig. 6, C and D). These mice exhibited normal testis histology with a full complement of spermatogenic cells in the seminiferous epithelium, but a few exceptions were noted. First, occasional apoptotic cells were found in the *Kdm4d*$^{-/-}$ tubules (Fig. 6, I and J). These apoptotic cells were detected in testes older than 10 wk, but their frequency was very low. Second, the tubule diameter was wider in *Kdm4d*$^{-/-}$ testes than in *Kdm4d*$^{+/-}$ testes at 3 wk, although no significant differences were found in tubule diameter in older mice (Fig. 6, E–J, and data not shown).

To determine the effect of KDM4D ablation on spermatocytes, H3K9me2/3 in *Kdm4d*$^{+/-}$ and *Kdm4d*$^{-/-}$ testicular cells were examined, because *Kdm4d* transcripts were expressed not only in spermatids but also in spermatocytes (Fig. 1C). No significant differences were found in level and distribution of H3K9me2 and H3K9me3 in zygotene and pachytene spermatocytes, indicating that lack of KDM4D did not affect meiotic progression in spermatocytes (Fig. 7).

During spermiogenesis, histone H4 can be hyperacetylated immediately before histone replacement to protamine, and its hyperacetylation is important for histone replacement [23]. Some reports have been published about correlations between methylated H3K9 and histone acetylation [24–27]. Thus, a histone acetylase, CDYL (chromodomain on Y chromosome like), and acetylated histone H3 and H4 were stained in *Kdm4d*$^{+/-}$ and *Kdm4d*$^{-/-}$ testis. CDYL was localized in germ cells in the center of the seminiferous tubule and was detected with higher expression in elongating spermatids. Acetylated histone H3 was localized to round spermatids and elongating spermatids, and strong immunoreactivity of acetylated H4 was detected in elongating spermatids. However, no significant changes were found in expression and distribution of CDYL, acetylated histone H3, and acetylated histone H4 (Supplemental Fig. S3), suggesting that acetylation of histones was not affected by lack of KDM4D-dependent demethylation of H3K9me3.

Because the jmjC domain of KDM4D shares more than 84% of identity with the jmjC domain of other KDM4 proteins [13, 14], other KDM4 proteins might have a redundant role with KDM4D in spermatogenesis. To evaluate this possibility, other KDM4 proteins were analyzed. We found that KDM4B was expressed during spermatogenesis, particularly in elongated spermatids (Fig. 8). Although expression of KDM4B was not changed between *Kdm4d*$^{+/-}$ mice and *Kdm4d*$^{-/-}$ mice at 10 wk of age, a difference was observed in testis at 25 days, when spermatids start to elongate. Whereas KDM4B was localized in the cytoplasm of elongating spermatids in 25-day-old testes of *Kdm4d*$^{+/-}$ mice, nuclear localization of KDM4B was detected in elongating spermatids of *Kdm4d*$^{-/-}$ mice (Fig. 8). These findings suggest that nuclear import of KDM4B could be promoted by loss of KDM4D to rescue a critical problem at the final step of spermatogenesis in *Kdm4d*$^{-/-}$ mice.

DISCUSSION

In the present report, we show, to our knowledge for the first time, the expression of KDM4D in multiple tissues. Although KDM4D expression is specific for testis in both the NCBI EST and BioGPS databases [20], KDM4D transcripts were detected not only in testis but also weakly in brain, lung, and kidney. However, the expression of KDM4D in tissues other than testis was very low. Because *Kdm4d* knockout mice are viable and no significant abnormalities are found in other tissues, KDM4D is not required extragonadally. However, it is still possible that KDM4D is redundant with other H3K9 tridemethylases [13, 14, 28–30]. To clarify the functions of KDM4D in those tissues, not only KDM4D but also other KDM4 family proteins need to be investigated.

Some, but not all, of the *Kdm4d*$^{-/-}$ testes were bigger than *Kdm4d*$^{+/-}$ testes during limited periods. This might be correlated with the differences in the diameter of tubules at 3

TABLE 1. Fertility testing of *Kdm4d*$^{+/-}$ and *Kdm4d*$^{-/-}$ males over nine months.

Genotype	n	Litters	Total pups	Pups/litter*	Litters/month*
Kdm4d$^{+/-}$	10	97	1062	9.77 ± 0.19	1.21 ± 0.01
Kdm4d$^{-/-}$	10	93	991	9.91 ± 0.21	1.19 ± 0.02

* Results are shown as the mean ± SEM.

Downloaded from www.biolreprod.org.

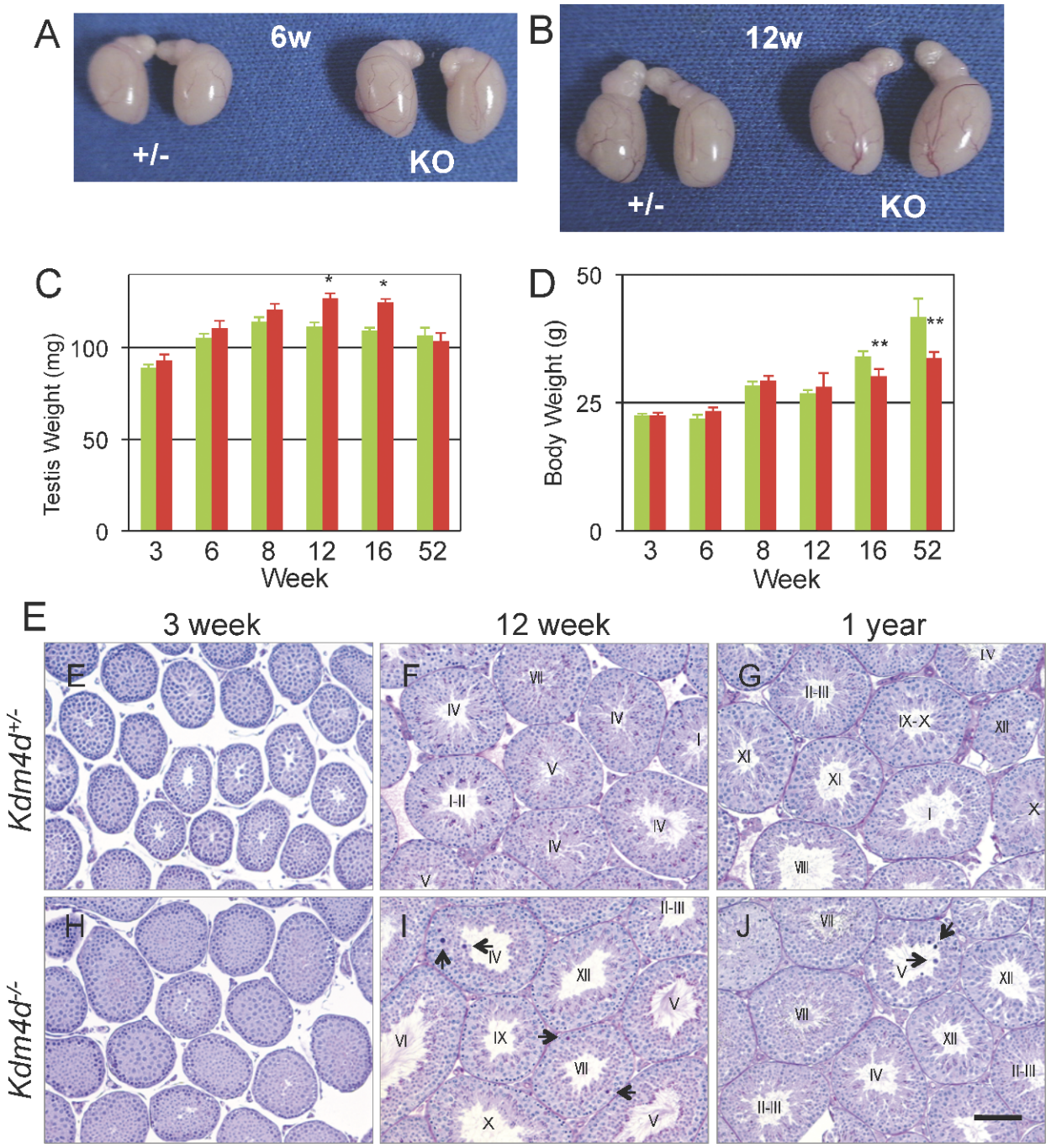

FIG. 6. Phenotype of *Kdm4d*$^{-/-}$ testes. **A** and **B**) Gross pictures of *Kdm4d*$^{+/-}$ (+/–) and *Kdm4d*$^{-/-}$ (KO) testes at 6 wk (**A**) and 12 wk (**B**) of age. **C** and **D**) Testis (**C**) and body (**D**) weights of *Kdm4d*$^{+/-}$ mice (green bar) and *Kdm4d*$^{-/-}$ mice (red bar) at indicated ages (n ≥ 5 mice). **E**–**J**) Histological analysis. Testes from *Kdm4d*$^{+/-}$ (**E**–**G**) and *Kdm4d*$^{-/-}$ (**H**–**J**) mice at 3 wk (**E** and **H**), 12 wk (**F** and **I**), and 1 yr (**G** and **J**) are shown. Roman numerals indicate spermatogenic stages. Arrows indicate apoptotic cells. *$P < 0.01$, **$P < 0.05$.

wk of age, although the sizes of *Kdm4d*$^{+/-}$ testis and *Kdm4d*$^{-/-}$ testis were not different. In contrast, no clear differences were found in the diameter of tubules at 12 wk of age, although *Kdm4d*$^{-/-}$ testes were significantly heavier than *Kdm4d*$^{+/-/-}$ testes. However, those differences appeared not to be essential for spermatogenesis, and no data explained these differences.

We have shown that KDM4D is involved in trimethylation/didemethylation of H3K9, consistent with previous experiments [13, 14]. However, the total amounts of H3K9me2 in testis were not changed by the *Kdm4d* deletion, although H3K9me3 was significantly increased in *Kdm4d*-null round spermatids. H3K9me2 in round spermatids was not high and was localized in the center of nuclei of wild-type round spermatids according to our results. However, nuclear foci of H3K9me2 disappeared in *Kdm4d*$^{-/-}$ round spermatids, even if H3K9me2 was detected in *Kdm4d*$^{-/-}$ round spermatids by immunoblot, suggesting that H3K9me2 could be broadly distributed in the nucleus at undetectable levels by immunostaining. In the first report of KDM3A mutant mice, although total amounts and distribution of H3K9me2 in testis were not significantly changed, H3K9me2 accumulated at specific sites, such as the promoter regions of *Prm1* and *Tnp1* [12]. The

Downloaded from www.biolreprod.org.

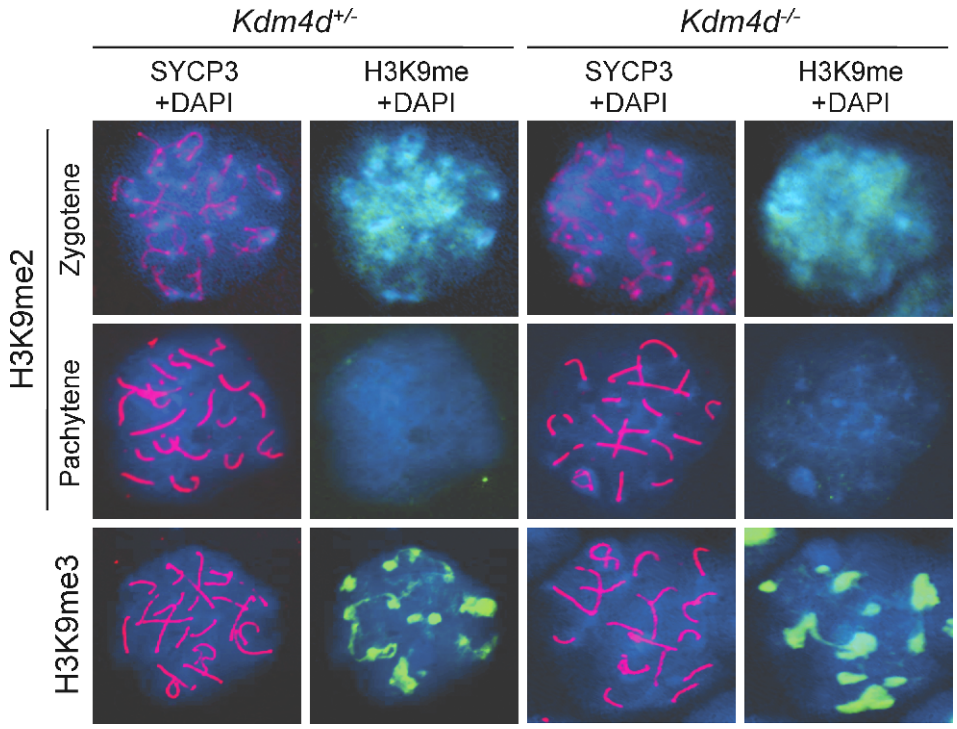

FIG. 7. Methylation of H3K9 in spermatocytes. *Kdm4d*$^{+/-}$ and *Kdm4d*$^{-/-}$ zygotene and pachytene spermatocytes were stained with anti-H3K9me2 or anti-H3K9me3 (green) and anti-SCP3 (red) antibodies and DAPI (blue). Images shown are merged images of each staining and DAPI.

second report of *Kdm3a* knockout mice showed an increase and change of distribution of H3K9me2 and H3K9me1 in testis [6]. Demethylation of H3K9me2, therefore, could be catalyzed by KDM3A/JHDM2A/JMJD1A expressed in round spermatids, and other didemethylases of H3K9 may participate in this process. KDM4D might regulate H3K9me2 at a specific region. However, our results indicate that foci of H3K9me2 in round spermatids disappeared in *Kdm4d*$^{-/-}$ round spermatids,

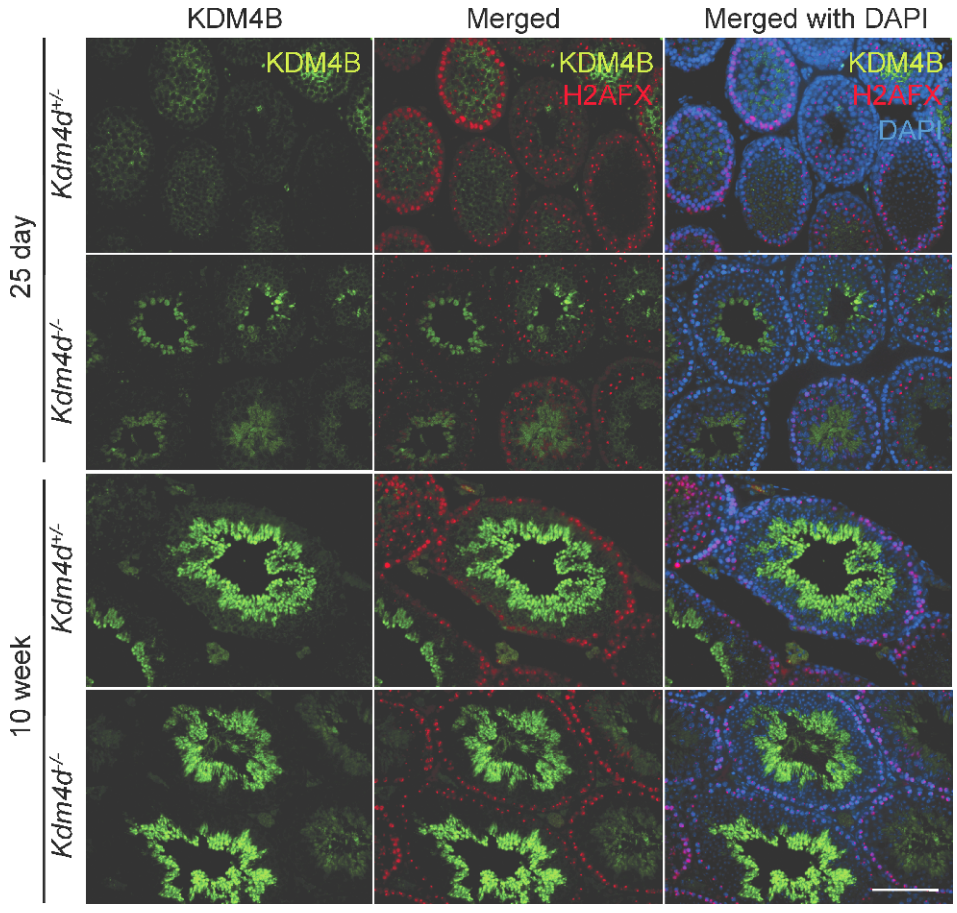

FIG. 8. Expression of KDM4B in *Kdm4d*$^{+/-}$ and *Kdm4d*$^{-/-}$ testes. Testes from *Kdm4d*$^{+/-}$ and *Kdm4d*$^{-/-}$ mice at 25 days and 10 wk of age were stained with anti-KDM4B (green), anti-H2AFX (red), and DAPI (blue).

Downloaded from www.biolreprod.org.

and simultaneously, H3K9me3 foci in round spermatids became stronger, suggesting that foci of H3K9me2 in round spermatids were converted from H3K9me3 by KDM4D. Because both H3K9me2 and H3K9me3 are repressive marks of transcription, there might not be big differences in transcriptional regulation between *Kdm4d*$^{+/-}$ and *Kdm4d*$^{-/-}$ round spermatids. Nevertheless, dramatic changes in the methylation status of H3K9 occur in *Kdm4d*$^{-/-}$ testis, and a variety of genes may be altered in their expression in *Kdm4d*$^{-/-}$ testis. Global gene expression profiles as well as analysis of KDM4D- and methylated H3K9-occupied loci in testis and/or in each specific germ cell type could help to define the roles of methylated H3K9 during not only normal spermatogenesis but also in the absence of KDM4D.

A relationship between H3K9me3 and acetylation of histone H4 during spermatogenesis has been suggested. H3K9me3 can be recognized by the chromodomain of HP1, and its binding is important for heterochromatin formation [31, 32]. Histone acetyltransferase, CDYL, has a chromodomain that is implicated in H3K9me3 binding and can acetylate histone H4 [24–27]. Histone H4 is hyperacetylated just before histone replacement to protamine [23, 33, 34]. CDYL could regulate acetylation of H4 in elongating spermatids according to the expression pattern of CDYL, although no direct evidence shows that CDYL could be responsible for hyperacetylation of histone H4 [24]. In *Kdm4d*$^{-/-}$ testis, localization of CDYL, acetylated histone H3, and acetylated histone H4 are normal, suggesting that hyperacetylation of histone H4 before histone replacement is not affected by lack of KDM4D.

Lastly, our results suggest that KDM4B could have redundant roles with KDM4D in *Kdm4d*$^{-/-}$ testis. Both KDM4D and KDM4B have a jmjC domain, which is responsible for demethylation activity [14, 28]. KDM4D has jmjN and jmjC domains, whereas KDM4B has not only jmjN and jmjC domains but also two Plant Homeo and two TUDOR domains. Plant Homeo and TUDOR domains may be important for binding to other proteins as well as for recognition of specific loci in the genome [14, 30]. Although KDM4D can demethylate not only H3K9me3 but also H3K9me2, KDM4B can demethylate H3K9me3 but not H3K9me2 [14, 30]. Furthermore, H3K9me3 demethylation activity of KDM4D was much stronger than that of KDM4B [14]. In our results, H3K9me2 is still detectable in *Kdm4d*$^{-/-}$ elongated spermatids, but H3K9me3 is not, suggesting that H3K9me3 in *Kdm4d*$^{-/-}$ elongated spermatids could be demethylated by KDM4B. Additionally, H3K9me2 remains in *Kdm4d*$^{-/-}$ elongated spermatids, because KDM4B could not catalyze H3K9me2. Alternatively, histones that have H3K9me2 could be removed earlier from chromatin in *Kdm4d*$^{+/-}$ elongated spermatids than in *Kdm4d*$^{-/-}$ elongated spermatids, because histone removal is already beginning at the elongating spermatid stage. Double knockout of KDM4D and KDM4B would be helpful to further define the roles of H3K9me3 demethylation during spermatogenesis as well as spermiogenesis.

ACKNOWLEDGMENT

We thank Dr. Tokuko Iwamori for her kind assistance in manuscript preparation.

REFERENCES

1. Nottke A, Colaiacovo MP, Shi Y. Developmental roles of the histone lysine demethylases. Development 2009; 136:879–889.
2. Shi Y. Histone lysine demethylases: emerging roles in development, physiology and disease. Nat Rev Genet 2007; 8:829–833.
3. Kouzarides T. Chromatin modifications and their function. Cell 2007; 128:693–705.
4. Mosammaparast N, Shi Y. Reversal of histone methylation: biochemical and molecular mechanisms of histone demethylases. Annu Rev Biochem 2010; 79:155–179.
5. Martin C, Zhang Y. The diverse functions of histone lysine methylation. Nat Rev Mol Cell Biol 2005; 6:838–849.
6. Liu Z, Zhou S, Liao L, Chen X, Meistrich M, Xu J. Jmjd1a demethylase-regulated histone modification is essential for cAMP-response element modulator-regulated gene expression and spermatogenesis. J Biol Chem 2010; 285:2758–2770.
7. Payne C, Braun RE. Histone lysine trimethylation exhibits a distinct perinuclear distribution in Plzf-expressing spermatogonia. Dev Biol 2006; 293:461–472.
8. Godmann M, Auger V, Ferraroni-Aguiar V, Di Sauro A, Sette C, Behr R, Kimmins S. Dynamic regulation of histone H3 methylation at lysine 4 in mammalian spermatogenesis. Biol Reprod 2007; 77:754–764.
9. Peters AH, O'Carroll D, Scherthan H, Mechtler K, Sauer S, Schofer C, Weipoltshammer K, Pagani M, Lachner M, Kohlmaier A, Opravil S, Doyle M, et al. Loss of the Suv39h histone methyltransferases impairs mammalian heterochromatin and genome stability. Cell 2001; 107:323–337.
10. O'Carroll D, Scherthan H, Peters AH, Opravil S, Haynes AR, Laible G, Rea S, Schmid M, Lebersorger A, Jerratsch M, Sattler L, Mattei MG, et al. Isolation and characterization of Suv39h2, a second histone H3 methyltransferase gene that displays testis-specific expression. Mol Cell Biol 2000; 20:9423–9433.
11. Tachibana M, Nozaki M, Takeda N, Shinkai Y. Functional dynamics of H3K9 methylation during meiotic prophase progression. EMBO J 2007; 26:3346–3359.
12. Okada Y, Scott G, Ray MK, Mishina Y, Zhang Y. Histone demethylase JHDM2A is critical for Tnp1 and Prm1 transcription and spermatogenesis. Nature 2007; 450:119–123.
13. Shin S, Janknecht R. Diversity within the JMJD2 histone demethylase family. Biochem Biophys Res Commun 2007; 353:973–977.
14. Whetstine JR, Nottke A, Lan F, Huarte M, Smolikov S, Chen Z, Spooner E, Li E, Zhang G, Colaiacovo M, Shi Y. Reversal of histone lysine trimethylation by the JMJD2 family of histone demethylases. Cell 2006; 125:467–481.
15. Liu P, Jenkins NA, Copeland NG. A highly efficient recombineering-based method for generating conditional knockout mutations. Genome Res 2003; 13:476–484.
16. Edson MA, Lin YN, Matzuk MM. Deletion of the novel oocyte-enriched gene, Gpr149, leads to increased fertility in mice. Endocrinology 2010; 151:358–368.
17. Adams DJ, Quail MA, Cox T, van der Weyden L, Gorick BD, Su Q, Chan WI, Davies R, Bonfield JK, Law F, Humphray S, Plumb B, et al. A genome-wide, end-sequenced 129Sv BAC library resource for targeting vector construction. Genomics 2005; 86:753–758.
18. Nalam RL, Lin YN, Matzuk MM. Testicular cell adhesion molecule 1 (TCAM1) is not essential for fertility. Mol Cell Endocrinol 2010; 315:246–253.
19. Peters AH, Plug AW, van Vugt MJ, de Boer P. A drying-down technique for the spreading of mammalian meiocytes from the male and female germline. Chromosome Res 1997; 5:66–68.
20. Su AI, Wiltshire T, Batalov S, Lapp H, Ching KA, Block D, Zhang J, Soden R, Hayakawa M, Kreiman G, Cooke MP, Walker JR, et al. A gene atlas of the mouse and human protein-encoding transcriptomes. Proc Natl Acad Sci U S A 2004; 101:6062–6067.
21. Meistrich ML. Separation of spermatogenic cells and nuclei from rodent testes. Methods Cell Biol 1977; 15:15–54.
22. Zhao M, Rohozinski J, Sharma M, Ju J, Braun RE, Bishop CE, Meistrich ML. Utp14b: a unique retrogene within a gene that has acquired multiple promoters and a specific function in spermatogenesis. Dev Biol 2007; 304:848–859.
23. Meistrich ML, Trostle-Weige PK, Lin R, Bhatnagar YM, Allis CD. Highly acetylated H4 is associated with histone displacement in rat spermatids. Mol Reprod Dev 1992; 31:170–181.
24. Lahn BT, Tang ZL, Zhou J, Barndt RJ, Parvinen M, Allis CD, Page DC. Previously uncharacterized histone acetyltransferases implicated in mammalian spermatogenesis. Proc Natl Acad Sci U S A 2002; 99:8707–8712.
25. Mulligan P, Westbrook TF, Ottinger M, Pavlova N, Chang B, Macia E, Shi YJ, Barretina J, Liu J, Howley PM, Elledge SJ, Shi Y. CDYL bridges REST and histone methyltransferases for gene repression and suppression of cellular transformation. Mol Cell 2008; 32:718–726.
26. Franz H, Mosch K, Soeroes S, Urlaub H, Fischle W. Multimerization and

Downloaded from www.biolreprod.org.

H3K9me3 binding are required for CDYL1b heterochromatin association. J Biol Chem 2009; 284:35049–35059.
27. Fischle W, Franz H, Jacobs SA, Allis CD, Khorasanizadeh S. Specificity of the chromodomain Y chromosome family of chromodomains for lysine-methylated ARK(S/T) motifs. J Biol Chem 2008; 283:19626–19635.
28. Klose RJ, Yamane K, Bae Y, Zhang D, Erdjument-Bromage H, Tempst P, Wong J, Zhang Y. The transcriptional repressor JHDM3A demethylates trimethyl histone H3 lysine 9 and lysine 36. Nature 2006; 442:312–316.
29. Chen Z, Zang J, Whetstine J, Hong X, Davrazou F, Kutateladze TG, Simpson M, Mao Q, Pan CH, Dai S, Hagman J, Hansen K, et al. Structural insights into histone demethylation by JMJD2 family members. Cell 2006; 125:691–702.
30. Fodor BD, Kubicek S, Yonezawa M, O'Sullivan RJ, Sengupta R, Perez-Burgos L, Opravil S, Mechtler K, Schotta G, Jenuwein T. Jmjd2b antagonizes H3K9 trimethylation at pericentric heterochromatin in mammalian cells. Genes Dev 2006; 20:1557–1562.
31. Bannister AJ, Zegerman P, Partridge JF, Miska EA, Thomas JO, Allshire RC, Kouzarides T. Selective recognition of methylated lysine 9 on histone H3 by the HP1 chromo domain. Nature 2001; 410:120–124.
32. Lachner M, O'Carroll D, Rea S, Mechtler K, Jenuwein T. Methylation of histone H3 lysine 9 creates a binding site for HP1 proteins. Nature 2001; 410:116–120.
33. Gaucher J, Reynoird N, Montellier E, Boussouar F, Rousseaux S, Khochbin S. From meiosis to postmeiotic events: the secrets of histone disappearance. FEBS J 2010; 277:599–604.
34. Grimes SR Jr, Henderson N. Hyperacetylation of histone H4 in rat testis spermatids. Exp Cell Res 1984; 152:91–97.

Downloaded from www.biolreprod.org.